Available online at www.sciencedirect.com
SCIENCE DIRECT®
International Journal of Heat and Fluid Flow 25 (2004) 659–670
International Journal of HEAT AND FLUID FLOW
www.elsevier.com/locate/ijhff

Numerical modeling of buoyancy-driven turbulent flows in enclosures

K.J. Hsieh, F.S. Lien *

Department of Mechanical Engineering, University of Waterloo, 200 University Avenue West, Waterloo, Ont., Canada N2L 3G1

Received 15 May 2003; accepted 30 November 2003
Available online 3 February 2004

Abstract

Modeling turbulent natural convection in enclosures with differentially heated vertical walls is numerically challenging, in particular, when low-Reynolds-number (low-*Re*) models are adopted. When the turbulence level in the core region of cavity is low, most low-*Re* models, particular those showing good performance for bypass transitional flows, tend to relaminarize the flow and, as a consequence, significantly underpredict the near-wall turbulence intensities and boundary-layer thickness. Another challenge associated with low-turbulence buoyancy-driven flows in enclosures is its inherent unsteadiness, which can pose convergence problems when a steady Reynolds-averaged Navier–Stokes (RANS) equation is solved. In the present study, an unsteady RANS approach in conjunction with the low-*Re* k–ϵ model of Lien and Leschziner [Int. J. Comput. Fluid Dyn. 12 (1999) 1] is initially adopted and the predicted flow field is found effectively relaminarized. To overcome this difficulty, likely caused by the low-*Re* functions in the ϵ-equation, the two-layer approach is attempted, in which ϵ is prescribed algebraically using the one-equation k–l model of Wolfshtein [Int. J. Heat Mass Transfer 12 (1969) 301]. The two-layer approach combined with a quadratic stress–strain relation gives overall the best performance in terms of mean velocities, temperature and turbulence quantities.

Keywords: Natural convection; Non-linear k–ϵ model; Unsteady RANS

1. Introduction

Natural convection in enclosures is encountered in many engineering applications, including cooling of electronic packages, solar collectors, and building ventilation. Numerous experimental and numerical studies have been conducted in the past, and most of them are concentrated in rectangular cavities because it represents one of the simplest geometries with many applications in industry.

Even though measurement techniques and numerical methods have improved significantly in the last decade, the investigation of turbulent natural convection remains very challenging. The low velocities are difficult to measure and ideal adiabatic wall conditions are hard to achieve. The strong coupling between flow and temperature fields and strong interaction between boundary-layers and core flow make computation very "stiff" and convergence difficult. In addition, the flow in a cavity, in particular for cooling of electronics, is likely to be transitional. This causes problems for most of the Reynolds-averaged Navier–Stokes (RANS)-based turbulence models, most of which were calibrated in fully turbulent flow conditions. To avoid 'relaminarization' caused by certain low-Reynolds-number (low-*Re*) models at moderate Rayleigh numbers ($Ra = 10^{10}$–10^{12}), the high-Reynolds-number (high-*Re*) k–ϵ model with variants of wall functions were selected as the 'mandatory model' in a Eurotherm workshop in 1992, focused on turbulent natural convection in enclosures with differentially heated vertical side walls (Henkes and Hoogendoorn, 1995). The experiment for a cavity of AR = 5 (AR is the aspect ratio) at $Ra = 5 \times 10^{10}$ conducted by Cheesewright et al. (1986) were chosen as the benchmark test problem. Henkes and Hoogendoorn summarized the results presented in the workshop and reported that the location of onset of transition was extremely sensitive to the streamwise grid density and such sensitivity could be avoided by triggering the transition in the boundary-layer

* Corresponding author. Tel.: +1-519-888-4567; fax: +1-519-888-6197.
E-mail addresses: khsieh@engmail.uwaterloo.ca (K.J. Hsieh), fslien@uwaterloo.ca, fslien@sunwise.uwaterloo.ca (F.S. Lien).

0142-727X/$ - see front matter © 2004 Elsevier Inc. All rights reserved.
doi:10.1016/j.ijheatfluidflow.2003.11.023

with a fixed amount of turbulence kinetic energy. Tieszen et al. (1998) computed the same test problem and found that the v^2–f model of Durbin (1995) also predicted a significant delay of onset of transition, yielding an underestimation of local Nusselt number. They overcame the relaminarization problem by including the buoyancy production term G_k with the turbulent heat flux modeled by Daly and Harlow's (1970) generalized gradient diffusion hypothesis (GGDH), which seemed to trigger the correct onset of transition. However, they also reported that the inclusion of G_k had very small effect on the results for the heated vertical plate test problem of Tsuji and Nagano (1988) using the same v^2–f model.

In addition to Cheesewright et al.'s experimental study for a cavity of AR = 5, the measurements of Tian and Karayiannis (2000) and Betts and Bokhari (2000) in air-filled cavities, with AR = 1 and 28.68, respectively, have also often been used as benchmark problems for turbulence model validation. For the square cavity of Tian and Karayiannis at $Ra = 10^9$, the flow in the core of cavity was quiescent and thermally stratified. Besides, turbulence was concentrated in the boundary-layers and its intensity level was *low*—an ideal test case for direct numerical simulation (DNS) and/or large eddy simulation (LES). Peng and Davidson (2001) and Ham (2002) used LES to study this flow. They employed Smagorinsky's (1963) eddy-viscosity model with its model constant C determined by the dynamic procedure of Germano et al. (1991). As expected, the predicted local Nusselt number, mean temperature field and turbulence quantities along the vertical walls agree very well with the experimental data.

However, low level of turbulence intensity can relaminarize the flow for certain type of low-*Re* k–ϵ models, such as the Launder–Sharma model (1974). For bypass transitional flows at $u'/U_\infty \gtrapprox 3\%$ (viz, the turbulence level is higher than that in Tian and Karayiannis's square cavity), this model was recommended by Savill (1993) as one of the best eddy-viscosity models investigated in a European Research Community on Flow Turbulence and Combustion (ERCOFTAC) Special Interest Group Project. The major drawback of Launder and Sharma's model is the extra source term $E = 2\nu\nu_t(\partial^2 u_i/\partial x_j \partial x_k)^2$ in the ϵ-equation, which is difficult to implement in 3-D general coordinate environment, and is highly sensitive to the near-wall grid resolution. To overcome this deficiency, Lien and Leschziner (1999) proposed a simpler low-*Re* k–ϵ model without the E term and demonstrated that performance of the model is similar to the Launder–Sharma model for bypass transitional flows. This model will be adopted in the present study to predict buoyancy-driven flows in cavities of different aspect ratios, in which transition might be an important issue.

To study turbulent convection in enclosures, Ince and Launder's model (1989) which is, in essence, the Launder–Sharma model combined with Yap's (1987) near-wall length-scale correction term in the ϵ-equation and buoyancy production term $G_k = -g_i\beta\overline{u_i'T'}$ in the k- and ϵ-equations, remains widely used due to its algorithmic simplicity and fairly good performance relative to more advanced k–ϵ–$\overline{\theta^2}$–ϵ_θ model of Hanjalic et al. (1996) and second-moment closure (e.g. Craft et al., 1996; Dol et al., 1999). In Tian and Karayiannis's case, where the turbulence level in the core region was low, Liu and Wen (1999) reported that the turbulence quantities along the vertical hot and cold walls as well as the boundary-layer thickness were significantly underpredicted by the Ince–Launder model. Interestingly, in the present study the Lien–Leschziner model, in conjunction with the Yap term in the ϵ-equation and the G_k term in the k- and ϵ-equations, also underpredicts the near-wall turbulence quantities and boundary-layer thickness (Section 4.2). Liu and Wen also attempted Hanjalic and Vasic's k–ϵ–$\overline{\theta^2}$ model (1993) and Hanjalic et al.'s k–ϵ–$\overline{\theta^2}$–ϵ_θ model and found that the results were still unsatisfactory: the peak values of turbulence quantities were better predicted, but the boundary-layer thickness was still too thin. In order to further improve the results, Liu and Wen added a second-order correction term, $\overline{u_i'u_j'}_{\mathrm{ASM}}$, to the Boussinesq linear stress–strain relationship in order to account for anisotropy of turbulence due to buoyancy, following the idea of Davidson (1990). They also proposed an ad hoc modification in the buoyancy production term in order to augment the shear stress generation rate and, hence, promote the transition.

It should be pointed out here that the k–ϵ–$\overline{\theta^2}$ model and the k–ϵ–$\overline{\theta^2}$–ϵ_θ model have the same ϵ-equation as in the Launder–Sharma model, which implies that, like the Ince–Launder model, could relaminarize the flow in Tian and Karayiannis's square cavity. In the present study, it was found that the two-layer approach (viz, combining the standard k–ϵ model in the core region with Wolfshtein's (1969) one-equation k–l model in the near-wall layers) with the interface located approximately at the peaks of velocities parallel to walls was able to trigger the onset of transition and promote the generation of turbulence. As a result, the predicted profiles of vertical velocity, horizontal and vertical turbulence intensities and temperature were greatly improved compared to the results obtained with the Lien–Leschziner model, which, like the Launder–Sharma model, tends to relaminarize the flow at low turbulence level.

The thermal boundary conditions on the upper and lower walls also have profound effect on the results. In Tian and Karayiannis's experiment, the temperature variations along the horizontal walls were not linear, i.e. the walls were not perfectly conducting. They recommended that the experimental temperature profile (ETP), as opposed to the linear temperature profile (LTP), be used as the boundary conditions in numerical

simulations. Both ETP and LTP were employed in the present study and, interestingly, we found that the Lien–Leschziner model performed quite well if LTP is used. The possible explanation for this will be discussed in Section 4.2.

Another challenge pertinent to buoyancy-driven flows in enclosures with low level of turbulence in the core region is the inherent unsteadiness, which poses severe convergence problems for steady RANS calculations, in particular, when higher-order convection schemes and fine meshes are adopted. In the present study, it is found necessary to use unsteady RANS to compute Tian and Karayiannis's flow. The results to be shown in Section 4.2 are time-averaged solutions and care has been taken to ensure that the results are independent on the grid sizes, time steps, averaging time and initial guessed flow fields.

In contrast, in the tall cavity case of Betts and Bokhari (2000) at $Ra = 10^6$, the flow was fully developed and turbulent but lacked thermal stratification at the cavity mid-height core region. The vertical turbulence intensity $v'/V_0 \approx 0.4$ in the core region at mid-height of the cavity is significantly higher than that of Tian and Karayiannis's flow, where $v'/V_0 \approx 0.06$. As a result, steady RANS can be used to compute this flow, and the onset of transition is predicted in the present study using the Lien–Leschziner model at $y/H \approx 0.1$ on the hot wall of the cavity. It is found that the inclusion of Yap term in the ϵ-equation is essential to predict correctly the horizontal profiles of vertical velocity and temperature. However, the average Nusselt number, $\overline{Nu}$, is much better represented by the model without the Yap term, which is consistent with Henkes and Hoogendoorn's (1995) observation for a vertical heated plate of Tsuji and Nagano (1988), in that the Launder–Sharma model with and without the Yap term underestimated wall heat transfer rate by 18% and 3%, respectively.

In what follows, the Lien–Leschziner model (1999), the quadratic stress–strain relationship of Speziale (1987) and Shih et al. (1993), two variants of turbulent heat flux model, and the two-layer approach based on the standard k–ϵ model and Wolfshtein's k–l model, are described in Section 2. Section 3 summarizes the main characteristics of Betts and Bokhari's (2000) and Tian and Karayiannis's (2000) experiments, the associated thermal boundary conditions and numerical method employed for the calculations to follow. Results and discussion are presented in Section 4, which allow conclusions to be drawn in Section 5.

2. Turbulence models

The governing equations, based on the low-Re k–ϵ model of Lien and Leschziner (1999) for natural convection flows, are

$$\frac{\partial u_i}{\partial t} + \frac{\partial}{\partial x_j}(u_j u_i) = -\frac{1}{\rho}\frac{\partial p}{\partial x_i} + \frac{\partial}{\partial x_j}\left[\nu\left(\frac{\partial u_i}{\partial x_j} + \frac{\partial u_j}{\partial x_i}\right) - \overline{u_i' u_j'}\right] - g_i\beta(T - T_{\mathrm{ref}}), \tag{1}$$

$$\frac{\partial T}{\partial t} + \frac{\partial}{\partial x_j}(u_j T) = \frac{\partial}{\partial x_j}\left[\frac{\nu}{Pr}\frac{\partial T}{\partial x_j} - \overline{u_j' T'}\right], \tag{2}$$

$$\frac{\partial k}{\partial t} + \frac{\partial}{\partial x_j}(u_j k) = \frac{\partial}{\partial x_j}\left[\left(\nu + \frac{\nu_t}{\sigma_k}\right)\frac{\partial k}{\partial x_j}\right] + (P_k + G_k) - \epsilon, \tag{3}$$

$$\frac{\partial \epsilon}{\partial t} + \frac{\partial}{\partial x_j}(u_j \epsilon) = \frac{\partial}{\partial x_j}\left[\left(\nu + \frac{\nu_t}{\sigma_\epsilon}\right)\frac{\partial \epsilon}{\partial x_j}\right] + \frac{\epsilon}{k}[C_{\epsilon 1}(P_k + P_k' + G_k) - C_{\epsilon 2}\epsilon] + \mathrm{Yap.}^{1} \tag{4}$$

The Boussinesq approximation is employed in the last term of Eq. (1) where $T_{\mathrm{ref}} = \frac{1}{2}(T_h + T_c)$ is a reference temperature, g_i is the gravitational acceleration vector, and β is the thermal expansion coefficient. The model constants σ_k, σ_ϵ, $C_{\epsilon 1}$, $C_{\epsilon 2}$ are

$$\sigma_k = 1, \quad \sigma_\epsilon = 1.3, \quad C_{\epsilon 1} = 1.44, \quad C_{\epsilon 2} = 1.92\left[1 - 0.3\exp(-R_t^2)\right], \tag{5}$$

where $R_t = \frac{k^2}{\nu\epsilon}$ is the local turbulent Reynolds-number,

$$P_k = -\overline{u_i' u_j'}\frac{\partial u_i}{\partial x_j}, \tag{6}$$

$$G_k = -g_i\beta\overline{u_i' T'}, \tag{7}$$

$$\mathrm{Yap} = \max\left[0.83\left(\frac{k^{3/2}}{2.5\epsilon l_n} - 1\right)\left(\frac{k^{3/2}}{2.5\epsilon l_n}\right)^2\frac{\epsilon^2}{k}, 0\right], \tag{8}$$

l_n in Eq. (8) denotes a wall-normal distance.

The P_k' in Eq. (4) was derived to ensure that the correct level of near-wall turbulence energy dissipation is returned, which is given as

$$P_k' = \frac{C_{\epsilon 2}}{C_{\epsilon 1}}\left(P_k + 2\nu\frac{k}{l_n^2}\right)\exp(-0.00375 l_n^{*2}), \tag{9}$$

where $l_n^* = l_n\sqrt{k}/\nu$.

2.1. Stress–strain relationship

Based on a series-expansion arguments (Pope, 1975), a general and co-ordinate invariant quadratic relationship between stresses and strains can be written as

[1] Note that one shortcoming of most low-Re k–ϵ models is that they tend to over-predict near-wall turbulence length scale. One remedy to overcome this problem, proposed by Yap (1987), is to introduce an extra source term defined in Eq. (8) into the ϵ-equation in order to adhere near-wall length scale ($k^{3/2}/\epsilon$) to its local equilibrium value.

$$\overline{u_i'u_j'} = \frac{2}{3}\delta_{ij}k - v_t\left(\frac{\partial u_i}{\partial x_j}+\frac{\partial u_j}{\partial x_i}\right) + f_\mu\frac{k^3}{\epsilon^2}\left[C_{\tau1}\left(\frac{\partial u_i}{\partial x_k}\frac{\partial u_j}{\partial x_k}\right)^* + C_{\tau2}\left(\frac{\partial u_i}{\partial x_k}\frac{\partial u_k}{\partial x_j}+\frac{\partial u_j}{\partial x_k}\frac{\partial u_k}{\partial x_i}\right)^* + C_{\tau3}\left(\frac{\partial u_k}{\partial x_i}\frac{\partial u_k}{\partial x_j}\right)^*\right], \tag{10}$$

where '*' indicates the deviatoric part; for example:

$$\left(\frac{\partial u_i}{\partial x_k}\frac{\partial u_j}{\partial x_k}\right)^* = \frac{\partial u_i}{\partial x_k}\frac{\partial u_j}{\partial x_k} - \frac{1}{3}\delta_{ij}\frac{\partial u_m}{\partial x_n}\frac{\partial u_m}{\partial x_n}. \tag{11}$$

The eddy-viscosity v_t in the k–ϵ modeling framework is

$$v_t = C_\mu f_\mu \frac{k^2}{\epsilon} \tag{12}$$

and the 'damping function', f_μ, in Eqs. (10) and (12), according to Lien and Leschziner (1999), is

$$f_\mu = [1-\exp(-0.0198l_n^*)]\left(1+\frac{5.29}{l_n^*}\right). \tag{13}$$

In the conventional *linear* eddy-viscosity model, $C_{\tau1}$, $C_{\tau2}$ and $C_{\tau3}$ are all zero, and $C_\mu = 0.09$. In the present study, these coefficients are chosen according to Speziale (1987) and Shih et al. (1993) as follows.

Speziale (1987):

$$(C_\mu, C_{\tau1}, C_{\tau2}, C_{\tau3}) = (0.09, 0.041, 0.014, -0.014). \tag{14}$$

Shih et al. (1993):

$$(C_\mu, C_{\tau1}, C_{\tau2}, C_{\tau3}) = \left(\frac{0.667}{1.25+S+0.9\Omega}, \frac{13}{1000+S^3}, \frac{-4}{1000+S^3}, \frac{-2}{1000+S^3}\right), \tag{15}$$

where $S = \frac{k}{\epsilon}\sqrt{S_{ij}S_{ij}/2}$, $\Omega = \frac{k}{\epsilon}\sqrt{\Omega_{ij}\Omega_{ij}/2}$, and

$$S_{ij} = \frac{\partial u_i}{\partial x_j}+\frac{\partial u_j}{\partial x_i}, \quad \Omega_{ij} = \frac{\partial u_i}{\partial x_j}-\frac{\partial u_j}{\partial x_i}. \tag{16}$$

2.2. Turbulent heat flux

There are two hypotheses commonly adopted to model the turbulent heat fluxes: the simple gradient diffusion hypothesis (SGDH) and the generalized gradient diffusion hypothesis (GGDH), defined below.

SGDH:

$$\overline{u_j'T'} = -\frac{v_t}{Pr_t}\frac{\partial T}{\partial x_j}. \tag{17}$$

GGDH:

$$\overline{u_j'T'} = -C_s\overline{u_j'u_k'}\frac{k}{\epsilon}\frac{\partial T}{\partial x_k}. \tag{18}$$

The SGDH is widely used in engineering application due to its simplicity. The SGDH assumes that the turbulent heat flux is proportional to the streamwise temperature gradient, where the turbulent Prandtl number (Pr_t) is around 0.9 in wall-bounded flows. Daly and Harlow (1970) first introduced the GGDH to account for the interaction between shear stress and spanwise temperature gradient. The GGDH expression was also adopted by Ince and Launder (1989) with $C_s = 0.3$ to model the G_k term in Eq. (7).

2.3. Two-layer approach

A hybrid approach of employing the one-equation k–l model of Wolfshtein (1969) in the 'inner' region and the standard high-*Re* k–ϵ model in the 'outer' region is also considered in the present study. The inner and outer regions are separated by the position of vertical velocity maximum (George and Capp, 1979). In the inner region, the eddy-viscosity v_t and ϵ are prescribed as

$$v_t = C_\mu 2.5 l_n D_v\sqrt{k} \tag{19}$$

and

$$\epsilon = \frac{k^{3/2}}{2.5 l_n D_\epsilon}, \tag{20}$$

where $C_\mu = 0.09$,

$$D_v = 1-\exp(-0.016l_n^*), \quad D_\epsilon = 1-\exp(-0.263l_n^*). \tag{21}$$

3. Problem definition and numerical details

3.1. Problem definition

The measurements of Tian and Karayiannis (2000) and Betts and Bokhari (2000) were conducted at a Rayleigh number based on the vertical wall temperature difference, $T_h - T_c$, and the cavity width, L $\left(\text{viz, } Ra = \frac{g\beta L^3(T_h-T_c)}{\nu\alpha}\right)$. Table 1 lists the configurations of both experiments.

3.2. Thermal boundary conditions

In the experiment of Betts and Bokhari, the horizontal walls were well insulted, and it is assumed that these walls are adiabatic in the present work. In contrast, the horizontal walls in the experiment of Tian and

Table 1
Configurations of the tall and square cavities

	Betts and Bokhari (2000)	Tian and Karayiannis (2000)
Cavity aspect ratio (AR = H/L)	28.68	1
Wall temperature difference	39.9 °C	40 °C
Rayleigh number	1.43×10^6	1.58×10^9

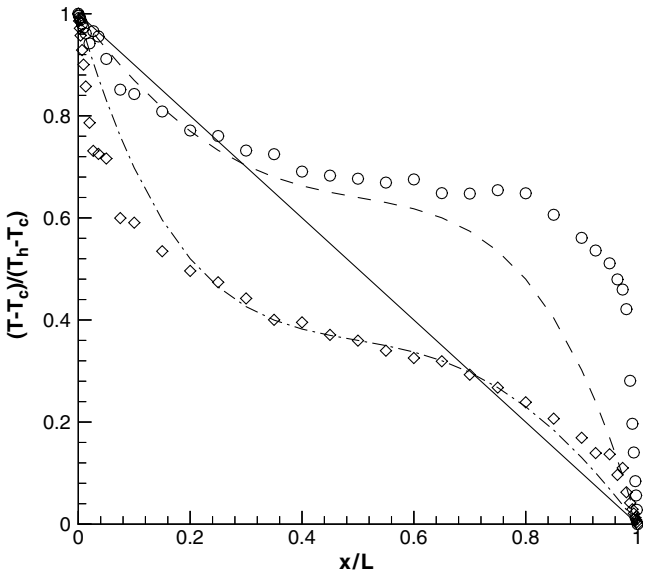

Fig. 1. Square cavity: experimental temperature profiles along the horizontal walls. — LTP; - - - ETP (top); – · – · – ETP (bottom); ○ expt (top); ◇ expt (bottom).

Karayiannis were highly conductive, and two different thermal boundary conditions are applied at these walls as shown in Fig. 1. The first one is to apply a linear temperature profile (LTP) between T_h and T_c assuming that the walls are perfectly conductive. The second one is to apply an experimental temperature profile (ETP), which is a best-fit polynomial based on the experimental data:

$$T = ax^4 + bx^3 + cx^2 + dx + e, \tag{22}$$

where the coefficients are listed in Table 2.

3.3. Numerical method

Calculations reported herein have been performed with the general non-orthogonal, fully collocated finite-volume approach STREAM (Lien and Leschziner, 1994a). Convection of mean-flow as well as turbulence quantities were approximated by the second-order TVD scheme 'UMIST' (Lien and Leschziner, 1994b). The transient term was discretized using a fully implicit, second-order accurate three-time-level method described in Ferziger and Peric (1999). The transport and the pressure-correction equations are solved sequentially and iterated to convergence by reference to Euclidean residual norms for mass and momentum components.

Table 2
Coefficients for the fitted polynomial curve described in Eq. (22)

	a	b	c	d	e
Top wall	−2.4583	1.6875	1.2108	−1.44	1
Bottom wall	2.4583	−8.1458	8.4767	−3.7892	1

For Tian and Karayiannis's square cavity, unsteady RANS was found necessary. The time-averaged quantities $\bar{\phi}$, including the local Nusselt number, mean-flow and turbulence quantities, were calculated by the following formula:

$$\bar{\phi} = \frac{1}{T}\int_{t_0}^{t_0+T} \phi \, \mathrm{d}t, \tag{23}$$

where $t_0 \approx 5000\Delta t$, and averaging time $T \approx 10,000\Delta t$. The time step $\Delta t \approx 0.25L/V_0$, where L is the width of the cavity and $V_0 = \sqrt{g\beta L(T_h - T_c)}$ is the buoyancy velocity. Different Δt, t_0 and T, initial guessed flow and turbulence fields, and a combination of them, have been tested to ensure that the final converged time-averaged results were attained. Hereafter the overbar sign of $\bar{\phi}$ will be removed for clarity in the following sections.

For the tall cavity flow of Betts and Bokhari (2000), where the turbulence level is high, steady RANS can be used and Δt was set to 10^{30} (viz, the unsteady term $\frac{\partial \phi}{\partial t} \to 0$).

4. Results and discussion

Results are presented for the following four model combinations described in Section 2, which are listed below preceded by identifiers used in plots and the related discussion:

(1) LL: k–ϵ model of Lien and Leschziner (1999) with linear stress–strain relationship;
(2) N-L LL: LL k–ϵ model above with Shih et al.'s stress–strain relationship defined in Eq. (15);
(3) 2-Layer: combining Wolfshtein's k–l model (1969) described in Section 2.3 in the inner region with linear high-Re k–ϵ model employed in the outer region;
(4) N-L 2-layer: 2-layer k–ϵ model above with Speziale's stress–strain relationship defined in Eq. (14). In this case, f_μ in Eq. (10) can be derived as (see Appendix A for details)

$$f_\mu = \frac{1 - \exp(-0.016 l_n^*)}{1 - \exp(-0.263 l_n^*)} \tag{24}$$

in order to be compatible with Wolfshtein's model.

The buoyancy velocity, $V_0 = \sqrt{g\beta L(T_h - T_c)}$, is used as a normalization parameter for the velocity and turbulence intensity results. The heat transfer rate along the wall expressed in terms of the local Nusselt number is defined as

$$Nu = -\frac{L}{T_h - T_c}\frac{\partial T}{\partial n}, \tag{25}$$

where n is the surface normal. The average Nusselt number ($\overline{Nu}$) along the heated vertical wall is calculated as:

$$\overline{Nu} = -\frac{\int_0^H Nu\,dy}{H}. \tag{26}$$

4.1. Tall cavity of Betts and Bokhari (2000)

To determine the accuracy of the numerical solutions, three grids of 50×100, 75×150, and 100×200 nodes are used. The only visible effect of grid refinement is on the onset of transition, which can be seen by the "trough" in the curve at $y/H \approx 0.1$ in Fig. 2. As the grid is refined, the transition is delayed, resulting in a slightly lower wall heat transfer rate as indicated in Table 3. Henkes and Hoogendoorn (1995) and Peng and Davidson (1999) also reported that the transition location in a rectangular cavity of AR = 5 (Cheesewright et al., 1986) was highly sensitive to grid refinement, which is consistent with the present observation.

Three different treatments of the buoyant term (G_k) are investigated in the preliminary study, namely the LL model with $G_k = 0$, with G_k modeled by SGDH, and with G_k modeled by GGDH. The predicted results from these three models are virtually identical (not shown), suggesting that buoyancy force is insignificant as a direct source of turbulence generation within the k–ϵ model framework. Tieszen et al. (1998) also reported that the effect of different buoyancy treatments on a flow over a heated vertical plate (Tsuji and Nagano, 1988), with solutions obtained with the v^2–f model of Durbin (1995), is small. The results presented hereafter are obtained using the finest grid and $G_k = 0$ unless stated otherwise.

As seen in Figs. 3 and 4, agreement between the LL model and the experimental data in terms of mean velocity and temperature profiles at four y/H locations

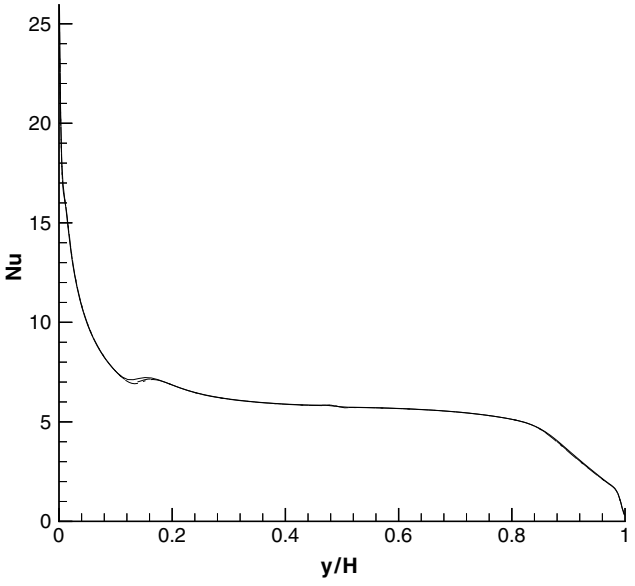

Fig. 2. Tall cavity: local Nusselt number distribution along the hot wall obtained with the LL model. — 50×100; - - - 75×150; – · – · – 100×200.

Table 3
Average Nusselt number results for the tall cavity

	$\overline{Nu}$
Experiment (Betts and Bokhari, 2000)	7.57
LL 50×100	6.01
LL 75×150	6.00
LL 100×200	5.99
N-L LL 100×200	6.39

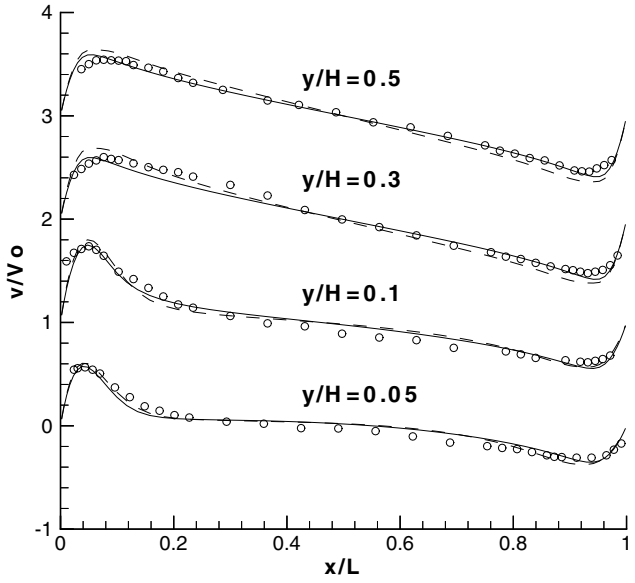

Fig. 3. Tall cavity: profiles of vertical velocity at four cavity heights. — LL; - - - N-L LL; ○ expt.

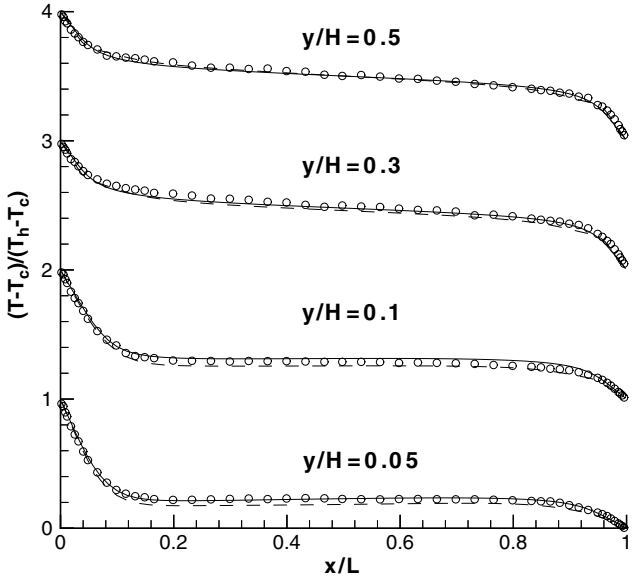

Fig. 4. Tall cavity: profiles of temperature at four cavity heights. — LL; - - - N-L LL; ○ expt.

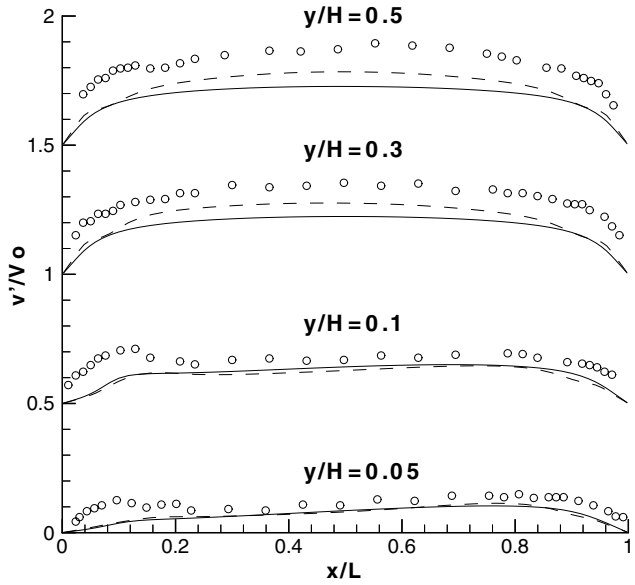

Fig. 5. Tall cavity: profiles of vertical turbulence intensity v' at four cavity heights. — LL; - - - N-L LL; ○ expt.

is fairly good, considering only a simple linear eddy-viscosity model is adopted here. However, discrepancy between the computed and measured turbulence intensity profiles is observed in Fig. 5, which is expected from almost any linear eddy-viscosity models. In contrast, the N-L LL model slightly over-predicts the velocity profiles and underpredicts the temperature profiles, but brings a significant improvement in the predicted turbulence intensities. At $y/H = 0.5$ in Fig. 5, the experimental data exhibits two troughs at $x/L = 0.16$ and $x/L = 0.85$, and the N-L LL model captures both troughs but at different locations: at $x/L = 0.08$ and $x/L = 0.92$. Similar features are also observed at three other cavity heights. It is concluded that the inclusion of the non-linear stress–strain relation yields higher turbulence intensity, which results in higher velocity and lower temperature predictions and, as a consequence, better predicted average Nusselt number, $\overline{Nu}$, shown in Table 3.

4.2. Square cavity of Tian and Karayiannis (2000)

The grid-independent study using the LL model in conjunction with the LTP thermal boundary condition on three different grids of 75×75, 100×100, and 125×125 nodes, is depicted in Fig. 6. As seen, very little difference can be observed in the local Nu distributions except near the peaks at $s/H \approx 0$ and $s/H \approx 2$, corresponding to the bottom of hot wall and top of the cold wall, respectively. The abscissa s/H denotes a length along the cavity walls in the clockwise direction, where $s/H = 0$ and $s/H = 4$ are at the left-bottom corner. When grids are refined, there is virtually no difference in Nu obtained with 100×100 and 125×125 nodes. The

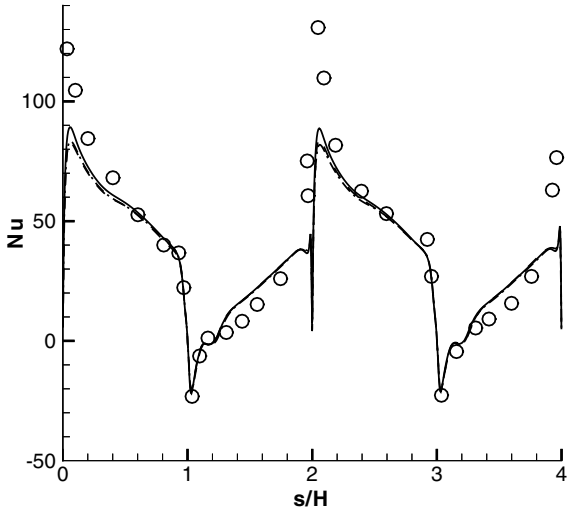

Fig. 6. Square cavity: local Nusselt number distribution obtained with the LL (LTP) model. — 75×75; - - - 100×100; – · – · – 125×125; ○ expt.

mesh of 125×125 nodes, therefore, supports grid-independent solutions, and is used henceforth to generate the results presented in this section.

Effect of different thermal boundary conditions, namely LTP and ETP described in Section 3.2, in conjunction with the LL model on the local Nusselt number and horizontal profiles of vertical velocity, temperature and turbulence quantities, including u'/V_0, v'/V_0 and $-\overline{u'v'}/V_0^2$, are displayed in Figs. 7–12. It is observed from Fig. 7 that LTP underpredicts the peak of Nu at $s/H = 0$ and 2 compared to those obtained with ETP, although both solutions are lower than the experimental values by about 30% for LTP and 16% for ETP, respectively. The possible explanation is given below by reference to Fig. 1, in which ETP on the bottom wall is

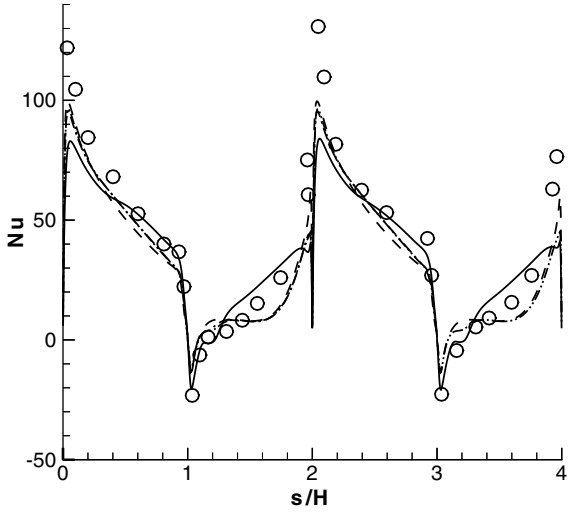

Fig. 7. Square cavity: local Nusselt number distribution. — LL (LTP); - - - LL (ETP); – · – · – 2-layer (ETP); – · · – N-L 2-layer (ETP); ○ expt.

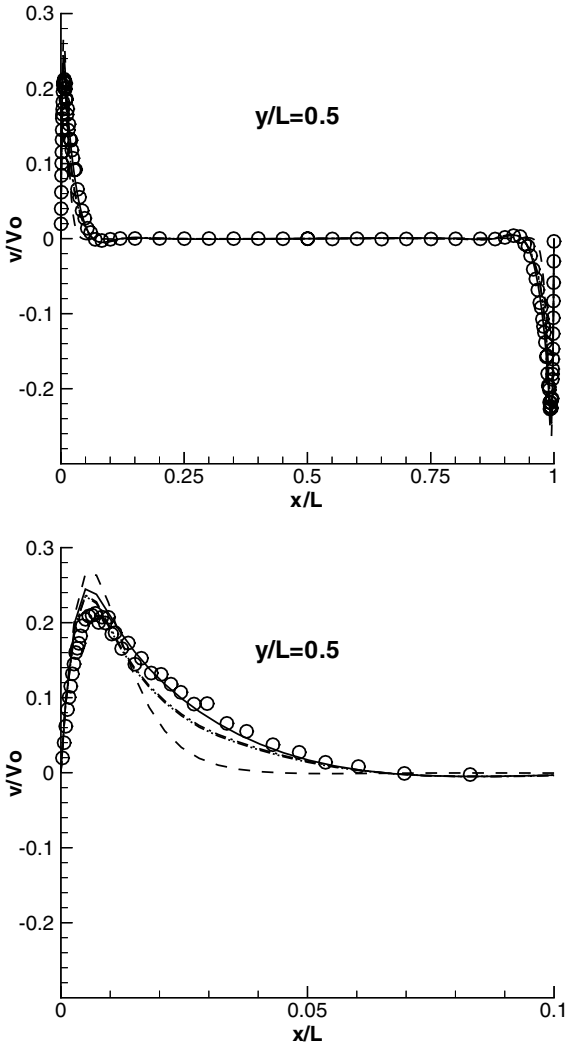

Fig. 8. Square cavity: profiles of vertical velocity at $y/L = 0.5$. — LL (LTP); - - - LL (ETP); – · – · – 2-layer (ETP); – · · · – N-L 2-layer (ETP); ○ expt.

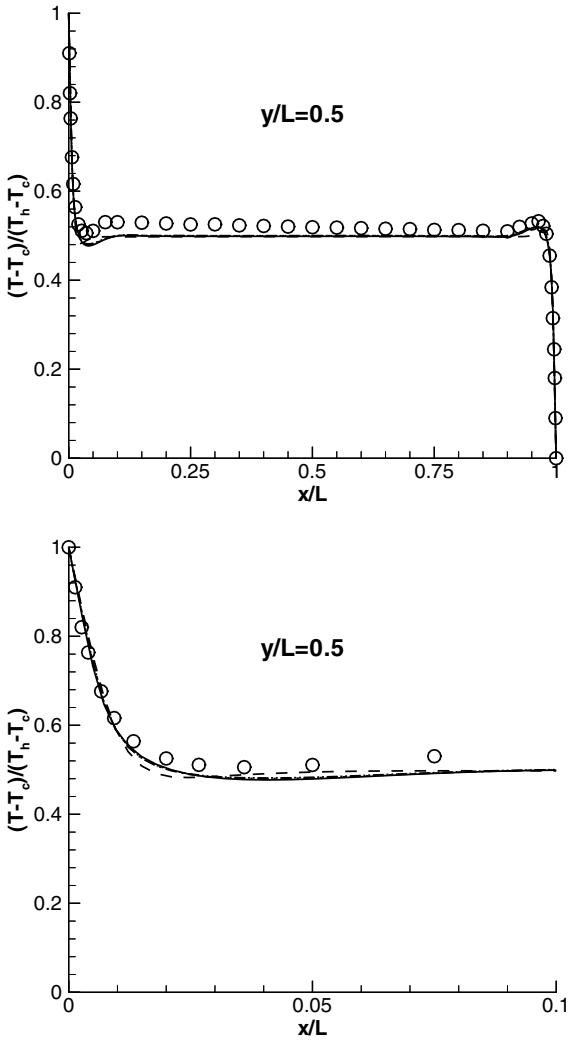

Fig. 9. Square cavity: profiles of temperature at $y/L = 0.5$. — LL (LTP); - - - LL (ETP); – · – · – 2-layer (ETP); – · · · – N-L 2-layer (ETP); ○ expt.

lower than LTP for $0 < x/L \lessapprox 0.7$. This implies that the buoyant force at the bottom-left corner of cavity produced by LTP is stronger than that by ETP. This not only reduces *Nu* at the corner due to a reduced level of temperature gradient there but, more importantly, promotes transition as is evident in Figs. 10–12, in which the boundary-layer thickness on both vertical walls and peaks of u'/V_0, v'/V_0 and $-\overline{u'v'}/V_0^2$ are better represented by LTP than by ETP. In fact, the LL model in conjunction with ETP tends to relaminarize the flow, as can be seen by the severe underprediction of peaks of all turbulence quantities shown in Figs. 10–12. This is consistent with Liu and Wen's observation when they adopted Ince and Launder's model for the same flow. In the present study, two variants of G_k described in Section 2.2, namely SGDH and GGDH, were also tested (not shown), resulting in no improvement in the results.

On the horizontal walls (viz, $1 \leqslant s/H \leqslant 2$ for the upper wall and $3 \leqslant s/H \leqslant 4$ for the lower wall), however, LTP overestimates *Nu* and ETP underestimates *Nu*, particularly in the middle portion of both upper and lower walls, in comparison with the experiment. It should be noted that the fourth-order polynomial fitting described in Eq. (22) and Table 2 to approximate the temperature variations along the upper and lower walls, though better than using LTP, is still unsatisfactory, in particular on the upper wall for $0.7 \lessapprox x/L < 1$. Different orders of polynomial were attempted (not shown) and their overall effect on the turbulence field was found to be insignificant.

As the failure of promoting transition seems to hinge on the low-*Re* functions, particularly those dependent on R_t, and wall-function-based models were reported by Henkes and Hoogendoorn (1995) to significantly overpredict the wall heat transfer rate, the 2-layer approach

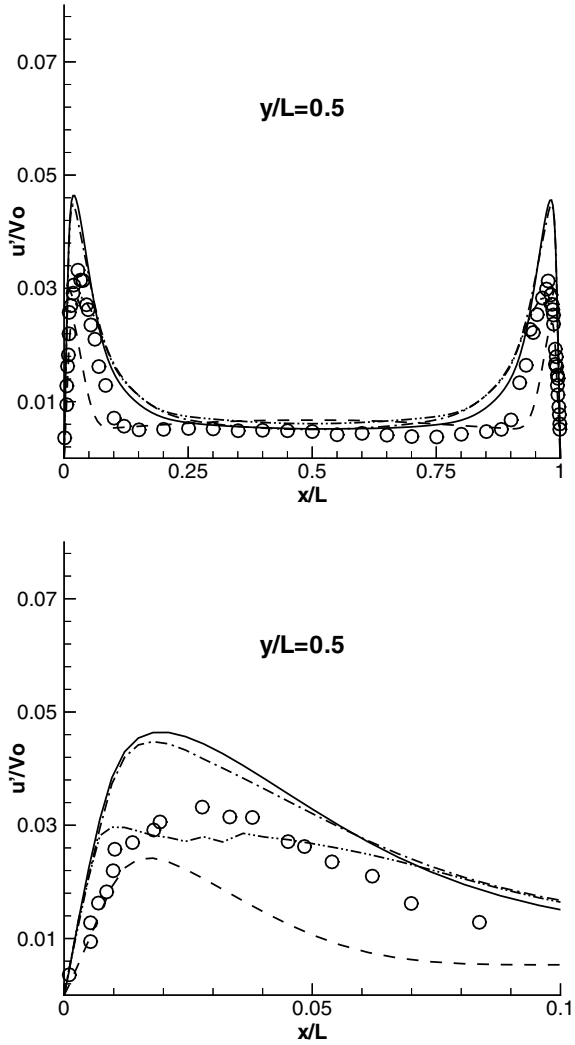

Fig. 10. Square cavity: profiles of horizontal turbulence intensity u' at $y/L = 0.5$. — LL (LTP); --- LL (ETP); –·–·– 2-layer (ETP); –··– N-L 2-layer (ETP); ○ expt.

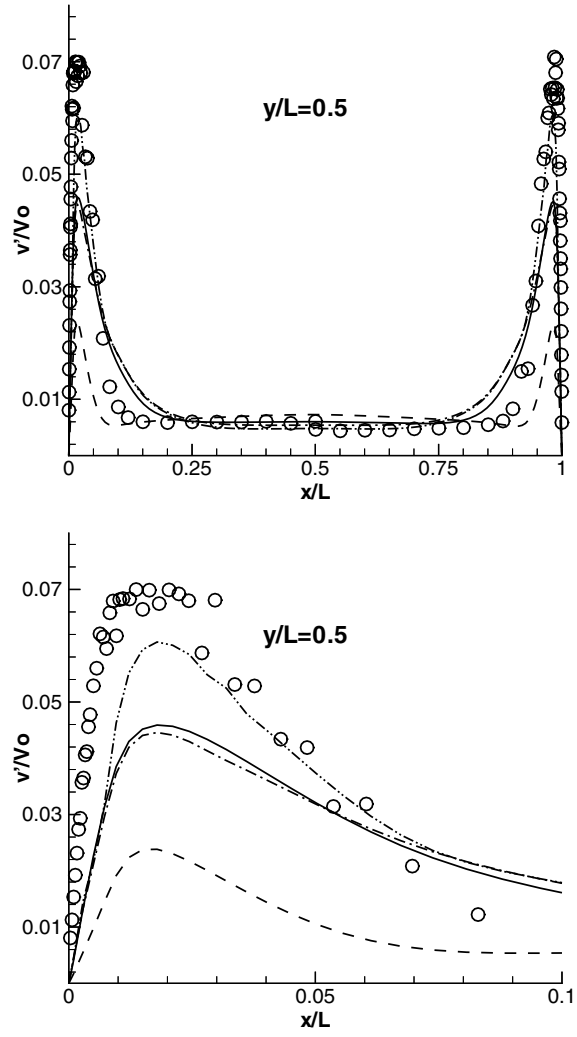

Fig. 11. Square cavity: profiles of vertical turbulence intensity v' at $y/L = 0.5$. — LL (LTP); --- LL (ETP); –·–·– 2-layer (ETP); –··– N-L 2-layer (ETP); ○ expt.

described in Section 2.3 were attempted here with the interface, separating the (inner) k–l near-wall model of Wolfshtein (1969) and the (outer) standard k–ϵ model, located at where the vertical velocity reaches its maximum. Typically, 8 to 12 nodes were placed in the inner region to ensure adequate near-wall grid resolution. Although the predicted Nu distributions by the LL (ETP) model and the 2-layer (ETP) model are quite similar as shown in Fig. 7, the 2-layer model does improve significantly the predicted turbulence profiles in the outer layer depicted in Figs. 10–12, particularly the $-\overline{u'v'}$ profile. Also the deficiencies of too thin boundary-layer thickness and too high velocity peak associated with the LL (ETP) model, observed in Fig. 8, were drastically improved when the 2-layer model is employed. However, the peak of u' is still over-predicted and the peak of v' underpredicted, as a consequence of employing the Boussinesq linear stress–strain relation. The locations of $u'_{\max}$ and $\overline{u'v'}_{\max}$ predicted by the LL (ETP) and 2-layer (ETP) models are both at $x/L \approx 0.02$, which are too close to the wall compared to the experimental observation where $x/L \approx 0.03$ (Figs. 10 and 12). However, the predicted locations of $v'_{\max}$ by both models are at $x/L \approx 0.02$, which agree quite well with the experimental value as seen in Fig. 11.

To properly account for the near-wall turbulence anisotropy within the present reasonably simple modeling framework without resorting to the k–ϵ–θ^2–ϵ_θ model of Hanjalic et al. (1996), the quadratic stress–strain relationship of Speziale (1987) with f_μ in Eq. (10) specifically derived in a manner compatible with the Wolfshtein's k–l model (see Appendix A) is also attempted here. As seen in Figs. 10 and 11, the turbulence anisotropy is much better represented by the N-L 2-layer model, although its effect on the predicted Nu

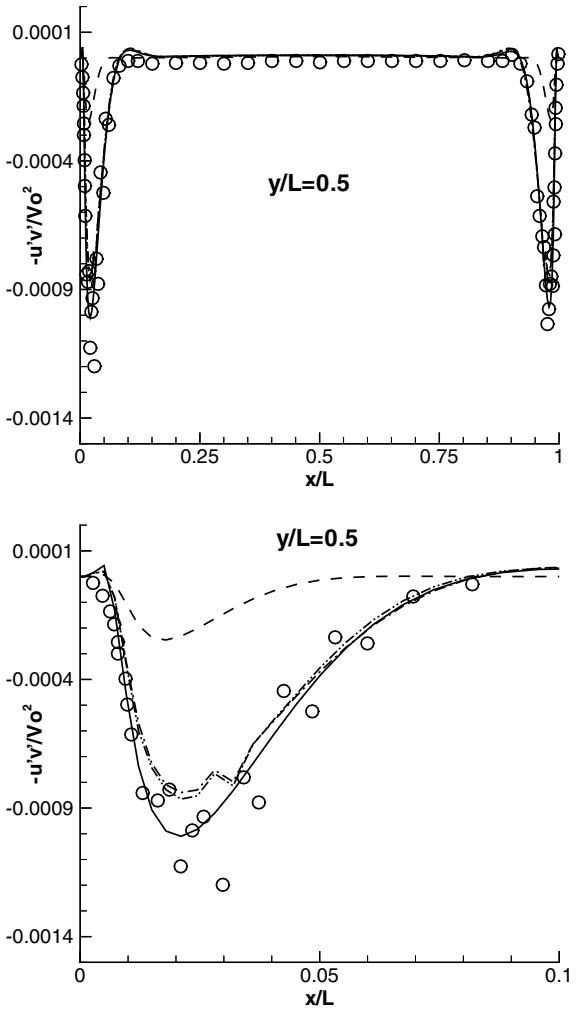

Fig. 12. Square cavity: profiles of turbulent shear stress $-\overline{u'v'}$ at $y/L = 0.5$. — LL (LTP); --- LL (ETP); –·–·– 2-layer (ETP); –··– N-L 2-layer (ETP); ○ expt.

distribution and velocity and temperature profiles, in contrast to the 2-layer model, is small.

The enlarged views ($0 \leqslant x/L \leqslant 0.1$) in Figs. 10–12 also display visible "kinks" particularly in u'- and $\overline{u'v'}$-profiles (not so much in v'-profile). The location of the kink is corresponding to the interface location separating the (inner) k–l model and the (outer) k–ϵ model—a well known defect associated with the 2-layer approach. Other than that, the rest part of the solutions are very smooth.

Finally, the average Nusselt number, $\overline{Nu}$, computed with four different model variants, namely the LL (LTP) model, the LL (ETP) model, the 2-layer (ETP) model and the N-L 2-layer (ETP) model are given in Table 4. It is seen from this table that the predicted $\overline{Nu}$ is in the range of 53.23 and 54.68 for all models investigated, suggesting that the 'conductive layer' (George and Capp, 1979) is relatively insensitive to which model was adopted. Interestingly, we underpredict $\overline{Nu}$ by approximately 17%, which is consistent with Henkes's (1990) study for a flow over a heated vertical plate, in which $\overline{Nu}$ was also underpredicted by 18% when the Launder–Sharma model with the Yap term was used.

Table 4
Average Nusselt number results for the square cavity

	$\overline{Nu}$ (Hot wall)	$\overline{Nu}$ (Cold wall)
Experiment (Tian and Karayiannis, 2000)	64.0	65.3
LL (LTP)	54.68	54.52
LL (ETP)	53.42	53.23
2-Layer (ETP)	54.50	54.51
N-L 2-layer (ETP)	54.60	54.60

5. Conclusions

The tall cavity of Betts and Bokhari (2000) at $Ra = 1.43 \times 10^6$ and the square cavity of Tian and Karayiannis (2000) at $Ra = 1.58 \times 10^9$ are investigated in the present study using variants of Lien and Leschziner's (LL) model and the two-layer approach. In the case of tall cavity, the performance of the LL model in terms of mean velocity and temperature profiles is generally fairly good compared to the experimental data. The average Nusselt number and profiles of vertical turbulence intensity can be further improved when the non-linear (quadratic) stress–strain relation of Shih et al. (1993) was employed. As the turbulence level in the core region is sufficiently high ($v'/V_0 \approx 0.4$), steady RANS can be used to compute this flow without encountering convergence problems.

In contrast, the turbulence level for the square cavity is quite low ($v'/V_0 \approx 0.06$) and unsteady RANS is deemed necessary to compute this flow. It is found that the thermal boundary conditions on the horizontal walls have profound effect on the predicted Nusselt number distributions. The LL (LTP) model underpredicts the peak values of Nusselt number. However, it promotes transition on the vertical walls, yielding solutions of velocity, temperature and turbulence quantities in good agreement with the experiment. When the LL (ETP) model is employed, the flow is effectively relaminarized regardless of whether G_k being included in the turbulence equations or not. To overcome this problem (a similar problem was reported by Liu and Wen (1999) to compute the same flow using Ince and Launder's model (1989)), a two-layer model was adopted, which, in conjunction with the non-linear stress–strain relation of Speziale (1987), drastically improves the predictions of mean-flow and turbulence fields. However, the average Nusselt number is still underpredicted, suggesting that more advanced turbulence models, such as second-moment closure, in conjunction with improved low-*Re*

functions in the ϵ-equation to avoid relaminarization, are required here.

Acknowledgements

The authors gratefully acknowledge the financial support from Materials and Manufacturing Ontario in Canada through MMO Project #DE708.

Appendix A

The eddy-viscosity expression arising from Wolfshtein's model, Eq. (19), can be rewritten as

$$v_t = C_\mu 2.5 l_n D_v \sqrt{k} = C_\mu 2.5 l_n D_v \left(\frac{k^{3/2}}{\epsilon}\right)^{-1} \frac{k^2}{\epsilon}. \tag{A.1}$$

Combining Eq. (20) with Eq. (A.1) gives us

$$v_t = C_\mu \frac{D_v}{D_\epsilon} \frac{k^2}{\epsilon}, \tag{A.2}$$

where D_v and D_ϵ are defined in Eq. (21). Comparing Eq. (A.2) with Eq. (12) allows us to derive the damping-function f_μ as

$$f_\mu = \frac{D_v}{D_\epsilon} = \frac{1 - \exp(-0.016 l_n^*)}{1 - \exp(-0.263 l_n^*)}. \tag{A.3}$$

References

Betts, P.L., Bokhari, I.H., 2000. Experiments on turbulent natural convection in an enclosed tall cavity. International Journal of Heat and Fluid Flow 21, 675–683.

Cheesewright, R., King, K.J., Ziai, S., 1986. Experimental data for the validation of computer codes for the prediction of two-dimensional buoyant cavity flow. Proceedings of the ASME Meeting, HTD, vol. 60, pp. 75–81.

Craft, T.J., Ince, N.Z., Launder, B.E., 1996. Recent developments in second-moment closure for buoyancy-affected flows. Dynamics of Atmospheres and Oceans 23, 99–114.

Daly, B.J., Harlow, F.H., 1970. Transport equations in turbulence. Physics of Fluids 13 (11), 2634–2649.

Davidson, L., 1990. Second-order corrections of the k–ϵ model to account for non-isotropic effects due to buoyancy. International Journal of Heat and Mass Transfer 33, 2599–2608.

Dol, H.S., Hanjalic, K., Versteegh, T.A.M., 1999. A DNS-based thermal second-moment closure for buoyant convection at vertical walls. Journal of Fluid Mechanics 391, 211–247.

Durbin, P.A., 1995. Separated flow computations with the k–ϵ–v^2 model. AIAA Journal 33, 659–664.

Ferziger, J.H., Peric, M., 1999. Computational Methods for Fluid Dynamics. Springer-Verlag, Berlin.

George, W.K., Capp, S.P., 1979. A theory for natural convection turbulent boundary layer next to heated surfaces. International Journal of Heat and Mass Transfer 22, 813–826.

Germano, M., Piomelli, U., Moin, P., Cabot, W., 1991. A dynamic subgrid-scale eddy viscosity model. Physics of Fluids A 3, 1760–1765.

Ham, F.E., 2002. Towards the large-eddy simulation of complex turbulent flows. Ph.D. thesis, University of Waterloo, Waterloo, Canada.

Hanjalic, K., Vasic, S., 1993. Computation of turbulent natural convection in rectangular enclosures with an algebraic flux model. International Journal of Heat and Mass Transfer 36, 3603–3624.

Hanjalic, K., Kenjeres, S., Durst, F., 1996. Natural convection in partitioned two-dimensional enclosures at higher Rayleigh numbers. International Journal of Heat and Mass Transfer 39, 1407–1427.

Henkes, R.A.W.M., 1990. Natural-convection boundary layers. Ph.D. thesis, Delft University of Technology, Delft, The Netherlands.

Henkes, R.A.W.M., Hoogendoorn, C.J., 1995. Comparison exercise for computations of turbulent natural convection in enclosures. Numerical Heat Transfer, Part B 28, 59–78.

Ince, N.Z., Launder, B.E., 1989. On the computation of buoyancy-driven turbulent flows in rectangular enclosures. International Journal of Heat and Fluid Flow 10 (2), 110–117.

Launder, B.E., Sharma, B.I., 1974. Application of the energy-dissipation model of turbulence to the calculation of flow near a spinning disk. Letters in Heat and Mass Transfer 1, 131–138.

Lien, F.S., Leschziner, M.A., 1994a. A general non-orthogonal collocated FV algorithm for turbulent flow at all speeds incorporating second-moment closure. Part 1: computational implementation. Computer Methods in Applied Mechanics and Engineering 114, 123–148.

Lien, F.S., Leschziner, M.A., 1994b. Upstream monotonic interpolation for scalar transport with application in complex turbulent flows. International Journal for Numerical Methods in Fluids 19, 527–548.

Lien, F.S., Leschziner, M.A., 1999. Computational modeling of a transitional 3D turbine-cascade flow using a modified low-*Re* k–ϵ model and a multi-block scheme. International Journal of Computational Fluid Dynamics 12, 1–15.

Liu, F., Wen, J.X., 1999. Development and validation of an advanced turbulence model for buoyancy driven flows in enclosures. International Journal of Heat and Mass Transfer 42, 3967–3981.

Peng, S.H., Davidson, L., 1999. Computation of turbulent buoyant flows in enclosures with low-Reynolds-number k–ω models. International Journal of Heat and Fluid Flow 20, 172–184.

Peng, S.H., Davidson, L., 2001. Large eddy simulation for turbulent buoyant flow in a confined cavity. International Journal of Heat and Fluid Flow 22, 323–331.

Pope, S.B., 1975. A more general effective-viscosity hypothesis. Journal of Fluid Mechanics 72, 331–340.

Savill, A.M., 1993. Further progress in the turbulence modeling of bypass transition. In: Rodi, W., Martelli, F. (Eds.), Engineering Turbulence Modelling and Experiments 2. Elsevier Science Publishers BV, pp. 583–592.

Shih, T.H., Zhu, J., Lumley, J.L., 1993. A realisable Reynolds stress algebraic equation model. NASA Technical Memorandum, 105993.

Smagorinsky, J., 1963. General circulation experiment with the primitive equation. I. The basic experiment. Monthly Weather Review 91, 99–165.

Speziale, C.G., 1987. On non-linear k–l and k–ϵ models of turbulence. Journal of Fluid Mechanics 178, 459–475.

Tian, Y.S., Karayiannis, T.G., 2000. Low turbulence natural convection in an air filled square cavity. Part I: the thermal and fluid flow fields. International Journal of Heat and Mass Transfer 43, 849–866.

Tieszen, S., Ooi, A., Durbin, P., Behnia, M., 1998. Modeling of natural convection heat transfer. Proceedings for the Summer Program 1998, Center for Turbulence Research, Stanford University, pp. 287–302.

Tsuji, T., Nagano, Y., 1988. Turbulence measurements in a natural convection boundary layer along a vertical flat plate. International Journal of Heat and Mass Transfer 31, 2101–2111.

Wolfshtein, M.W., 1969. The velocity and temperature distribution in one-dimensional flow with turbulence augmentation and pressure gradient. International Journal of Heat and Mass Transfer 12, 301–318.

Yap, C., 1987. Turbulent heat and momentum transfer in recirculating and impinging flows. Ph.D. thesis, Faculty of Technology, University of Manchester, UK.